Dynamics of the edge barrier collapse in intrinsic and pellet triggered ELMs

P.T. Lang, L. Fattorini[1], S. Kálvin[2], G. Kocsis[2], M.E. Manso[1], M.Maraschek,
J. Neuhauser, W.Suttrop, ASDEX Upgrade Team

Max-Planck-Institut für Plasmaphysik, EURATOM Association,
Boltzmannstr. 2, 85748 Garching, Germany
[1] *Centro de Fusão Nuclear, Associação EURATOM/IST, Instituto Superior Técnico,*
P-1049-001 Lisboa, Portugal
[2]*KFKI-RMKI, EURATOM Association, P.O. Box 49, H-1525 Budapest-114, Hungary*

Aim and procedure of the investigation

A promising solution to the type-I ELM power load problem in ITER is ELM pacing by pellets, as demonstrated experimentally on ASDEX Upgrade [1]. Extrapolation of this technique to ITER requires detailed knowledge about the basic physics involved in ELM onset, non-linear evolution and barrier collapse, and also about possible differences between pellet induced and spontaneous ELMs. In principle, a typical ELM evolution may be subdivided into several phases, e.g. a precursor phase with some increasing spikes and/or coherent mode activity, the main highly non-linear electromagnetic ELM phase accompanied by rapid edge energy and particle loss, and finally a slow recovery phase until again some precursor activity develops before the next ELM. A pellet launched during the more or less quiescent recovery phase produces a high pressure plasmoid layer, which is supposed to act as an externally induced artificial seed precursor triggering an ELM well before the next spontaneous one would appear. While the pellet plasmoid formation and dynamics has been well documented [2], the related ELM trigger mechanism and the barrier collapse modification have not yet been analysed in sufficient detail. An attempt to improve this situation is presented in the following.

In order to facilitate the analysis, we used specifically adapted discharge and pellet parameters: a stable type-I ELMy H-mode regime with low intrinsic ELM frequency $f_{ELM}^0 \approx 50$ Hz, established by adjusting the heating power above, but close to the H-mode threshold (typically $I_P = 1$ MA, 5 MW NBI auxiliary heating, $q_{95} = 4.9$). In addition, smallest (nominally $1.7 \times 10^{20}D$) and slowest (240 m/s) pellets were used with $f_{Pel} = 10$ Hz $< f_{ELM}^0$. Pellets were launched from the torus high-field side (HFS) relying on the existing centrifuge based fuelling system. With these settings, still each pellet is triggering an ELM at any time during the intrinsic ELM cycle, while the instantaneous density perturbation and the integral fuelling effect are small (perturbative trigger). In addition, the low pellet velocity expands the pedestal penetration time scale and allows to determine the radial position where the pellet perturbation is most effective for ELM release.

To characterize the precursor seed perturbation, the ELM signatures and the barrier collapse, specific fast edge diagnostics were studied simultaneously. Toroidal and poloidal magnetic pick-up coil arrays are recorded with a temporal resolution of 0.5 μs. The electron temperature is obtained at 32 μs resolution for the LFS employing ECE radiometry. Electron density collapse phases both at the LFS and HFS are characterized by reflectometry with a profile sweep and hence resolution time of 35 μs. Two analysis approaches were applied, one determining the evolution of the density gradient ∇n_e the other by tracking the motion of a certain density layer via the group delay τ_g of the according frequency [3]. A set of diodes recorded the D_α radiation from various regions, e.g. from the outer divertor strike line, sampled with 25 μs, and a specific pellet ablation monitor diode with 2 μs sampling, viewing the whole pellet injection path.

Results

A specific experimental problem in detailed ELM analysis is the strong variance of spontaneous as well as induced ELMs. Forming an average over many ELMs of a certain class tends to smooth away many interesting details, while a detailed analysis of a small number individual ELMs may not be sufficiently representative. Whatever approach is applied, a key element in the present context is to define a characteristic event within the ELM history, which can serve as a sufficiently accurate reference marker to compare the time evolution of different ELMs on a 10 μs scale. In fact, for the strong type-I ELMs investigated here, the onset of the MHD activity recorded by the magnetic pick-up coils turns out to satisfy our requirements. This is shown in figure 1 for a single ELM. Time traces from four representative magnetic pick-up coils around the torus are displayed in comparison to the pellet monitor signal and the divertor D_α radiation. The dB/dt signal increases rapidly on all magnetic probes at any position in the torus within about 20 μs. This can be quantitatively explained by the fast shear Alfvén wave communication along magnetic field lines, transmitting the initial magnetic seed perturbation, wherever started, all around the torus. For instance, assuming an Alfvén velocity of 5×10^6 m/s and a safety factor $q \sim 5$ somewhere in the edge pedestal, the magnetic perturbation travels five times around the torus in 10 μs and in parallel once around the plasma in poloidal direction. Taking into account the radial plasmoid extension and the radial magnetic shear, the magnetic wake has closely passed all pick-up coils during this short time interval. In this context, one should keep in mind that Alfvén and electron thermal velocity are of similar order in the plasma edge. Therefore, a strong local temperature perturbation, as in case of pellet injection, is communicated toroidally on the same time scale, while the sound speed is nearly two orders of magnitude slower. The pellet ablation monitor visualizes the increasing perturbation starting already when the pellet reaches the vicinity of the separatrix. At the time indicated the pellet has travelled already 4 cm inside the separatrix and it is thought here the ELM seed perturbation is launched. The enhanced D_α radiation from the outer divertor region monitors the delayed divertor response to the ELM induced breakdown of the edge transport barrier.
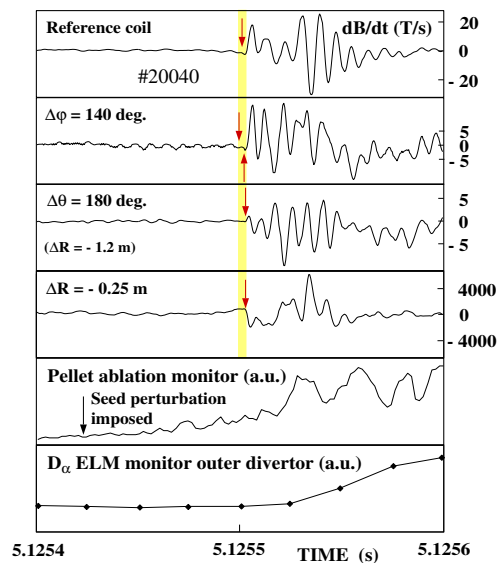
Figure 1: Time traces recorded for a typical single ELM (details see text).
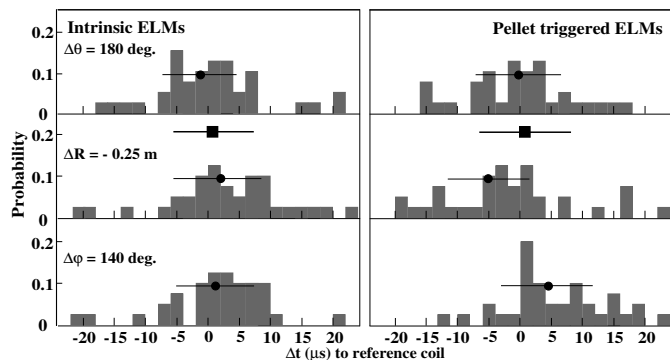
Figure 2: Distribution of MHD ELM onset times with respect to a reference coils for maximum poloidal, (almost) maximum toroidal and maximum available radial distance. Averaged time delay for each individual coil (circles) and any of these three coils (squares) are displayed for both kinds of ELMs.

ELM onset times for 36 reasonable events (negligible background MHD activity) each for pellet triggered and intrinsic ELMs were derived for the 4 representative coils, the time variation with respect to the reference one is plotted as histogram in figure 2. It shows obviously there is no significant difference between intrinsic and triggered ELMs becoming MHD visible on the Alfvén wave timescale everywhere at the plasma edge. The onset delay of any of these coils with respect to the reference one is 0.8 ± 9.6 μs for triggered and 0.6 ± 9.0 μs for intrinsic ELMs. In parallel, a detailed study of the ELM trigger mechanism by pellets has been done, using a quite different algorithm for onset time determination [4]. In general, the findings agree quite well. But as reported in [4], in at least a few shots analysed, there is a tendency for the HFS Mirnov coils to yield an earlier signal onset, roughly at a time when the pellet has just crossed the separatrix. Though the scatter is quite large, the effect seems to be statistically significant. We suppose that this earlier signal rise is related to the HFS pellet seed perturbation initiating the subsequent ELM, but this needs to be investigated in more detail.

Given the ELM onset time marker as defined above, we analyzed the breakdown of the transport barrier using the available fast diagnostics. Examples for single ELM events are displayed for both ELM types in figure 3. In the pellet case again the pre-ELM perturbation is clearly visible, the flight time required from the separatrix to the seed launch position is indicated. The breakdown of the transport barrier soon after the ELM MHD onset results in a drop of the edge electron temperature, an erosion of the steep density gradient and an enhancement of the density fluctuations in this region. The rapidly increasing outflux of particles and energy into SOL and divertor drives the divertor radiation. As might be expected for a spontaneous ELM, the MHD ELM onset time marks the very beginning of any significant edge parameter modifications. In fact, all other measured quantities related to the barrier become visible only several 10 μs (or one sampling interval) after ELM onset. Again the time at which a change is observed in these quantities has been statistically analysed (figure 4). The data shown were derived only from ELM events for which a complete set of edge measurements was available (22 intrinsic, 4 triggered). Due to limited storage capacity, reflectometer data can be recorded at highest temporal resolution only for 0.1 s (including typically a single pellet triggered ELM). To define the $t \equiv 0$ MHD ELM onset we determined the earliest time at which ELM MHD activity was detected in any of the coils, all other plotted values refer to this time marker. Black dots and diamonds represent averaged values for the diagnostic signal onset for intrinsic and triggered events, respectively. The time axis is vertically upward and time=0 corresponds to the MHD marker. Thin black lines represent the data scatter (FWHM), thick grey bars indicate the diagnostics temporal resolution. Grey boxes mark reflectometry results (density gradient and group delay) on HFS and LFS, respectively. It is seen that, roughly speaking, the barrier has started to collapse within less than 100 μs after the first indication of the ELM onset. Looking in more detail, the rise of the temperature perturbation and the divertor radiation is clearly delayed relative to the onset (T_e given for intrinsic ELMs only since not sufficient data were available for triggered ones, but analysis of additional cases indicates both types are rather similar). There is, however, at best a slight delay of the density profiles collapse for intrinsic ELMs and a somewhat larger for the triggered ones. In addition, the LFS density seems to respond a bit more promptly.

To understand these results in more detail, we have to take into account the communication from some local, initial seed perturbation around the torus to the respective diagnostic locations, as discussed earlier for the electromagnetic shear Alfvén wave. The

fast electron cooling wave (travelling on a similar time scale as the Alfvén wave) to be expected for the pellet case nearly in coincidence with the magnetic onset has not been identified so far within this specific data set and remains to be analysed. On the other hand, the early onset of the density perturbations at HFS and LFS, surprising at first glance, might be qualitatively consistent with the much smaller sound wave communication along field lines: for the pellet case, the field line length from the HFS injection point to the respective HFS and LFS reflectometry antennae typically corresponds to one toroidal revolution, i.e. a delay of order 100 μs. Keeping in mind that the pellet ablation starts about this amount of time before the ELM onset, it is troublesome to disentangle clearly pellet deposition and ELM effects. In case of an intrinsic ELM the approximate coincidence of density drop and magnetic ELM onset signal is less clear. In principle, the driving electromagnetic modes are supposed to cause some density perturbation in parallel to the magnetic field perturbation, but the diagnostic response at a specific point might depend on the detailed mode characteristics, which are not well known.
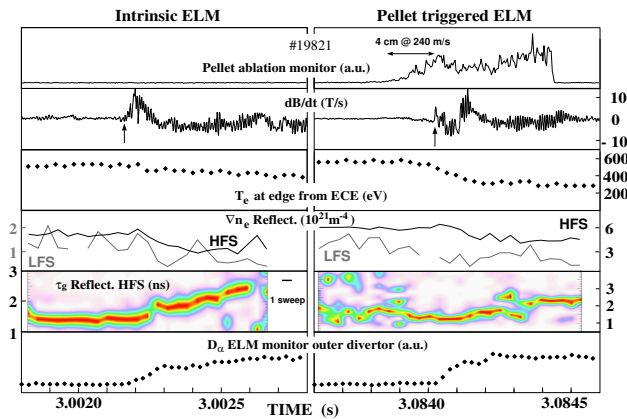
Figure 3: Intrinsic (left) and pellet induced (right) ELM. The ELM indicated by rapid MHD activity onset is accompanied by a breakdown of the edge transport barrier as indicated by the drop in edge density and temperature. The resulting particle and energy pulse to the divertor causes the observed D_α radiation.
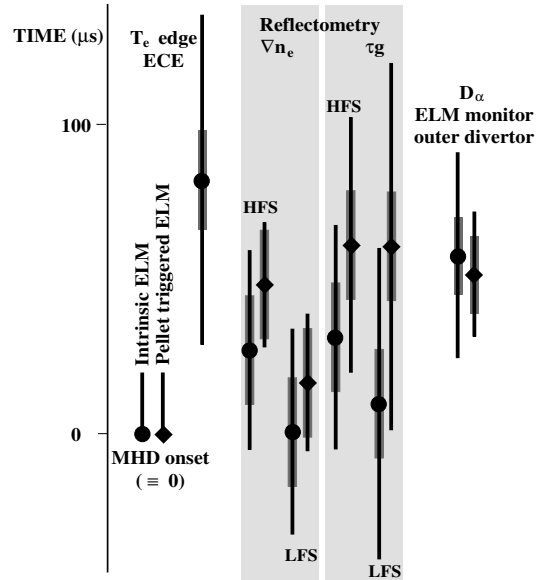
Figure 4: ELM appearance relative to first MHD onset ($\equiv$ 0) for intrinsic (dots) and pellet induced ELMs (diamonds). Thin black lines: data scatter, thick grey bars: temporal resolution.

Further experiments with improved temporal and spatial resolution allowing better separation of the processes in the ELM sequence are required. A new LFS pellet injection system will be employed to inject smaller and slower pellets. In addition, there is a chance for higher time resolution of key diagnostics by upgrading the data acquisition hardware.

References

[1] Lang, P.T. et al., Nucl. Fusion **43** (2003) 1110.
[2] Müller, H.W. et al., Phys. Rev. Lett. **83** (1999) 2199.
[3] Fattorini, L. et al., 32nd EPS conference (2005) P5.089.
[4] Kocsis, G. et al., this conference, P2.133.